



# 1 **Development of an integrated analytical platform of clay minerals** 2 **separation, characterization and $^{40}\text{K}/^{40}\text{Ar}$ dating**

3 Marie Gerardin<sup>1</sup>, Gaetan Milesi<sup>1</sup>, Julien Mercadier<sup>1</sup>, Michel Cathelineau<sup>1</sup>, Danièle Bartier<sup>1</sup>

4 <sup>1</sup>Université de Lorraine, CNRS, GeoRessources, 54520 Nancy, France

5 *Correspondence to:* Marie Gerardin (marie.gerardin@univ-lorraine.fr)

6 **Abstract.** Isotopic dating is a valuable method to constrain the timing of lithospheric processes: geodynamic episodes, ore  
7 deposition and geothermal regimes. The K-Ar dating technique has the main advantage of being applied to ubiquitous K-  
8 bearing minerals that crystallize in various temperatures, from magmatic to low temperatures. Clays are of significant interest  
9 among all K-bearing minerals, as they crystallize during various hydro-thermo-dynamic processes. Nonetheless, the dating of  
10 illites by the K-Ar method is not straightforward. K-Ar dates on illite usually rely on a mixed isotopic signal referring to  
11 various illitic populations that might have experienced isotopic resetting or re-crystallization processes. Therefore, reliable K-  
12 Ar dates on illite depend on (1) the grain size separation of large amounts of clay fractions, (2) the study of the morphology,  
13 mineralogy and crystallography, (3) the determination of precise K-Ar dates on each clay size fraction and (4) the meaningful  
14 interpretation of ages using either end-member ages or the Illite-Age-Analysis (IAA) method. This paper describes the  
15 instrumentation and methods recently developed at the GeoRessources laboratory of the University of Lorraine to obtain  
16 valuable ages on illite mixtures.

## 17 **1 Introduction**

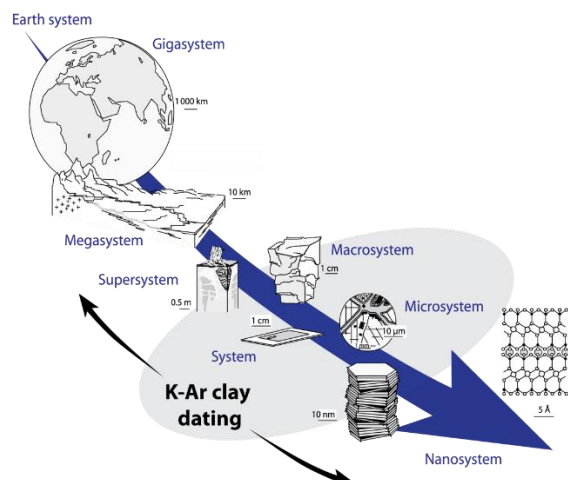
18 The K-Ar dating method is based on the principle of the natural radioactive decay of the parent element  $^{40}\text{K}$  to the daughter  
19 element  $^{40}\text{Ar}$ . Potassium is an abundant element in the lithosphere. Its half-life of  $1.248 \pm 0.004$  Ga (Steiger and Jäger, 1977;  
20 Grau Malonda and Grau Carles, 2002) is optimal for dating events over a wide range of geological times, from the early  
21 Precambrian to the Holocene (Dalrymple and Lanphere, 1969; Renne, 2000). Its abundance allows for detectable radiogenic  
22 argon accumulated after only several thousands of years. Argon is a noble gas, thus weakly bound to the mineral structure, but  
23 is retained in minerals because of its large atomic size (McDougall and Harrison, 1999, 1988). After sample melting, argon is  
24 measured by mass spectrometry (greatly developed after Nier's pioneering work in the 50's (Aldrich and Nier, 1948; Nier,  
25 1940, 1950)). The application to many rock-forming minerals, the large range of geological times explored, and the reliability  
26 of the quantitative determination of K and  $^{40}\text{Ar}$  make the K-Ar a popular dating technique developed worldwide. The early  
27 development of the K-Ar dating technique is extensively detailed in Schaeffer and Zähringer (1966) or in Dalrymple and  
28 Lanphere (1969). More recently, Guillou et al. (2021) provided an extensive review of the protocol and method along with its



29  $^{40}\text{Ar}/^{39}\text{Ar}$  derived version (fully described by McDougall and Harrison (1988)). Although the fundamentals of the method are  
30 not reiterated here, some key considerations are highlighted for a clear understanding of this work.

31 The method relies on several basic assumptions. (1) The decay of the parent nuclide,  $^{40}\text{K}$ , is not affected by temperature or  
32 pressure changes, (2) the  $^{40}\text{K}/\text{K}$  ratio (0.01167%) is constant over geological times, (3) the total amount of radiogenic  $^{40}\text{Ar}$   
33 measured in the mineral is produced by the decay of  $^{40}\text{K}$ , (4) the isotopic ratios of atmospheric argon remained unchanged  
34 over geological times (Renne et al., 2009) and (5) the mineral or rock evolved as a closed system that did not loss or gain  
35 potassium or radiogenic argon (other than by radioactive decay). The latter might be hypothetical if the system has a complex  
36 geological and thermal history, but the resulting age can still provide valuable information on the thermal history, especially  
37 by using the Ar-Ar step-heating technique (McDougall and Harrison, 1988) (more details about the comparison of K-Ar and  
38 Ar-Ar ages on illite can be found in Clauer et al. (2012)). Given these assumptions, the age calculated indicates the length of  
39 time the daughter element has remained trapped in the mineral. This age is then related to a crystallization event (cooling  
40 below the closure temperature) or recrystallization during more recent geological hydrothermal or thermal episodes.

41 The main advantage of the K-Ar method is its application on K-rich minerals like phyllosilicates or feldspars, which crystallize  
42 in a wide range of temperatures from low (100-300°C) to magmatic temperatures. Clay-type phyllosilicates are of particular  
43 interest considering their ubiquity at the scale of the Earth system (Fig. 1). Since their chemistry depends on physical conditions  
44 (pressure and temperature) and on the type of host rocks, clay minerals are helpful markers of low-temperature geological  
45 processes such as basin diagenesis (Perry, 1974; Meunier et al., 2004), low-temperature metamorphism (Reuter and Dallmeyer,  
46 1989; Akker et al., 2021), brittle fault deformation (Kralik et al., 1987; Monié et al., 2023) or hydrothermalism (Zwingmann  
47 et al., 1998; Brockamp and Clauer, 2013). The study of clay minerals, including their geochronology, is a powerful tool to  
48 constrain physical and chemical processes occurring at the micro- and nanoscale, improving our understanding of the evolution  
49 of the Earth system (Fig. 1).



50

51 **Fig. 1 – Potential of the K-Ar clay dating for the understanding of geological processes at different scale modified after (Velde and**  
52 **Meunier, 2008)**



53 One of the main concern about clay minerals dating is the interpretation of their ages, since the data result often from a mixture  
54 of different clay populations (broadly mentioned in Clauer's work, (Clauer, 2020a, b) for the latest), which could be affected  
55 by partial isotopic and chemical resetting or by a recurrent crystallization history. As clearly explained in Clauer (2020a) and  
56 Hueck et al. (2022) latest reviews, K-Ar dating should only be performed on illite fractions properly separated by grain size.  
57 Mineralogical, morphological, crystallographic and geochemical information are also required prior to dating to interpret the  
58 ages. Those conditions substantiate the need to develop an integrated method coupling efficient clay separations and  
59 characterization with K-Ar dating.  
60 This paper presents the platform developed at the GeoResources laboratory (University of Lorraine) to date clay minerals  
61 using the K-Ar method. It includes (1) a detailed description of the argon desorption line and its technical characteristics along  
62 with the methodology to quantify radiogenic argon and (2) the specificity of the separation protocol and the characterization  
63 steps necessary to obtain valuable ages on illites. Finally, the method to extrapolate ages from illite mixed populations is  
64 presented and discussed in the light of literature data.

## 65 **2 Description of the Argon desorption line and Methodology**

### 66 **2.1 Age calculation**

67 The K-Ar age calculation is based on two separately determined analytical values, the content of potassium ( $^{40}\text{K}$ , radioactive  
68 parent) and of radiogenic argon ( $^{40}\text{Ar}^*$ , radioactive daughter). Both analyses are destructive, therefore, two separate aliquots  
69 from the same sample are used. The homogeneity of these aliquots is granted by (1) preparing the two aliquots on the same  
70 day (same temperature and humidity conditions) and (2) using a large mass of aliquots to neglect the mineral heterogeneities.  
71 Classically, 100 mg is required for  $\% \text{K}_2\text{O}$  determination by absorption spectroscopy, regardless of the age or potassium  
72 content. For argon measurements, the mass minimum depends on the age and the argon content. A minimum of 1 to 3 mg is  
73 required for the clay fractions ( $<2\mu\text{m}$ ) and 20 mg for materials with larger particle sizes (see 0 for details about mass accepted  
74 in the desorption line).

75 The equation to calculate the age is derived from the fundamental law of radioactive decay and is expressed as follows:

$$t [\text{Ma}] = \frac{1}{\lambda} \ln \left( 1 + \frac{\lambda}{\lambda_\epsilon + \lambda'_\epsilon} \frac{n_S^{40^* \text{Ar}}(t) [\text{at/g}]}{n_S^{40\text{K}}(t) [\text{at/g}]} \right) \times 10^{-6} \quad (1)$$

76 where  $t$  is the age expressed in million annus (Ma) (Nomade, 2017),  $n_S^{40^* \text{Ar}}(t)$  is the number of atoms of  $^{40}\text{Ar}^*$  of argon per  
77 gram of sample at a time  $t$ ,  $n_S^{40\text{K}}(t)$  is the number of atoms of the radioactive  $^{40}\text{K}$  per gram of sample at a time  $t$  and  $\lambda$  is the  
78 total decay constant of  $^{40}\text{K}$  equal to  $\lambda_\epsilon + \lambda'_\epsilon + \lambda_\beta$  (see Table 1 listing the values and descriptions of constants used for the age  
79 calculation).



80 **Table 1 – Decay constants of  $^{40}\text{K}$  and isotopic abundances of K and Ar.**

Decay	Decay factor	Value	Reference
$^{40}\text{K}$ to $^{40}\text{Ca}$ by $\beta^-$	$\lambda_\beta$	$(4.96 \pm 0.11) \times 10^{-10}$	(Steiger and Jäger, 1977)
$^{40}\text{K}$ to $^{40}\text{Ar}$ by electron capture	$\lambda_\epsilon + \lambda'_\epsilon$	$(5.81 \pm 0.01) \times 10^{-11}$	
Isotopic abundances	Description	Value	Reference
% ( $^{40}\text{K}/\text{K}$ )	Isotope 40 of potassium	0.01167%	(Garner et al., 1975)
% ( $^{40}\text{Ar}/\text{Ar}$ )	Isotope 40 of argon	99.60%	(Lee et al., 2006)

81 **2.2 Measurement of the  $\text{K}_2\text{O}$  content**

82 The potassium content is determined by optical emission spectrometry (ICP-OES) at the SARM (Service d'Analyse des Roches  
83 et des Minéraux) of the CRPG laboratory at Nancy, France. The reliability of their measurements is based on repeatable  
84 experiments on standard materials. The uncertainty on  $\text{K}_2\text{O}$  expressed in weight % in the 1-10% quantity range (typical of  
85 micas) is about 1.5% for 100mg samples.

86 **2.3 Description of the desorption line for argon quantification**

87 Argon desorption is performed on an extraction-purification noble gas line. Preparation line specifications depend on each  
88 laboratory (Boulesteix et al., 2020; Cattani et al., 2019; Charbit et al., 1998a; Gillot and Cornette, 1986; Morgan et al., 2011;  
89 Phillips et al., 2017; Rouchon et al., 2008) but commonly comprise an induction furnace connected to a gas purification zone  
90 connected to a mass spectrometer. A schematic diagram of the ultra-high vacuum line developed at GeoRessources is shown  
91 in Fig. 2.

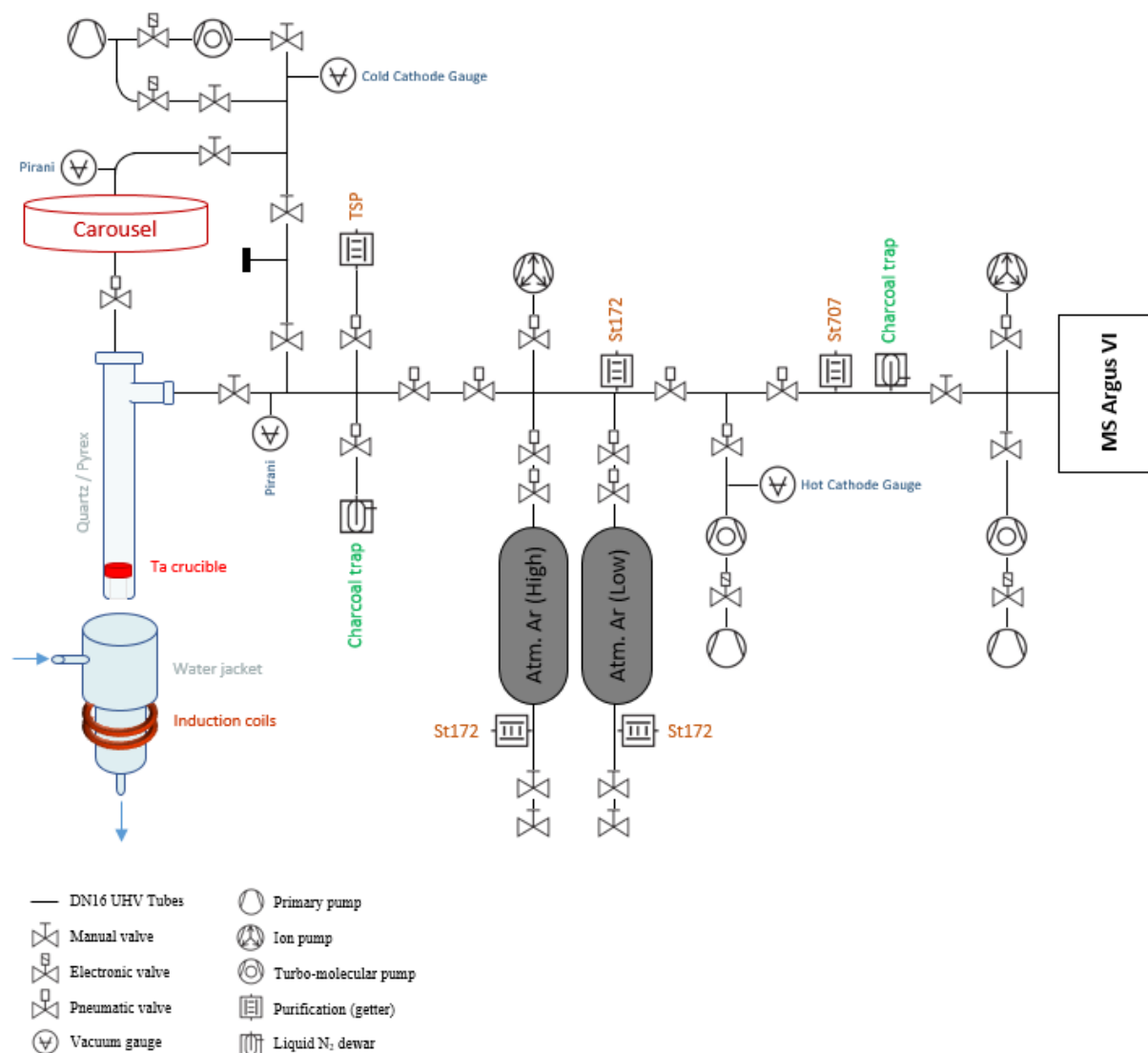


**Fig. 2 – Schematic representation of the argon desorption line from the induction furnace to the mass spectrometer**

92 Aliquots of samples are packed in a bending consisting of a 99.95% pure copper foil. They are placed under vacuum in  
 93 individual pits of the carousel above the furnace. The samples are vacuum pumped using a turbo-molecular pump during 24h.  
 94 This procedure was found to be equivalent to 24h backing at 105°C to remove adsorbed water from the sample (see 0).  
 95 Each of the ten pits connects to the furnace aperture by manual rotation of the carousel, dropping the sample by gravity into  
 96 the Ta crucible. The carousel is isolated from the furnace by an UHV gate valve during heating.  
 97 The heating-melting setup is identical to the one originally settled in LSCE (Guillou et al., 2021) and in GEOPS (Gillot and  
 98 Cornette, 1986) (Paris, France) for K-Ar dating. The samples are heated using a high-frequency furnace, the induction coil  
 99 ringing a quartz tube containing a Ta crucible mounted on a Mo stool (to avoid direct contact with the quartz tube).  
 100  
 101

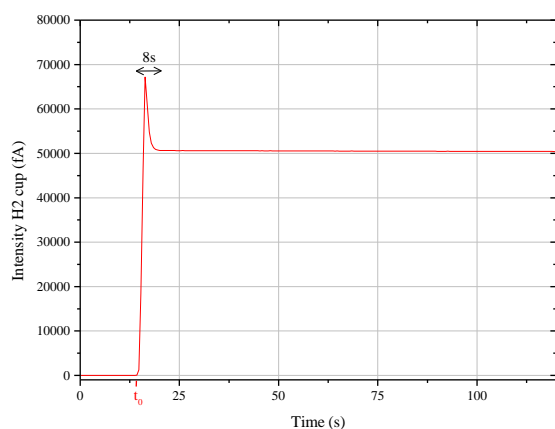


102 Gases other than argon that are released during powder melting could be water vapor, hydrogen, oxygen, nitrogen,  
103 hydrocarbons, and rare gases such as helium or krypton. The purification line next to the furnace is designed to trap all these  
104 gases in order to introduce only purified argon into the mass-spectrometer. The purification process is a two stage one, firstly  
105 extracted gases are exposed to a Ti sublimation pump and secondly to a GP50 SorbAC coupled to a St707 cartridge from  
106 SAES Getter operating at room temperature (see performance in Guillou et al., 2021). A charcoal trap cooled at  $-196^{\circ}\text{C}$  (liquid  
107 nitrogen temperature) is used to transfer the gas from the furnace through the purification line. This cold trap is also useful for  
108 gases separation since H and He are not physio-sorbed on the charcoal surface. The efficiency of the purification is checked  
109 for each sample (see section 2.5).

110 After 45 minutes of gas clean-up, Ar isotopes 36, 38 and 40 are simultaneously analyzed using an ARGUS VI multi-collector  
111 mass spectrometer, that is a magnetic mass sector with a Nier-type source designed for operation in a static mode (Mark et al.,  
112 2009). The ARGUS VI spectrometer has 5 Faraday detectors and one CDD detector. Argon 40 is measured on the H2 Faraday  
113 cup fitted with a  $10^{11}$  ohm resistor. Argon isotopes 36 and 38 are measured on the AX and the L2 cups respectively, both  
114 amplified with  $10^{12}$  ohm resistors. All collectors are cross-calibrated by scanning the  $^{40}\text{Ar}$  signal onto each cup. To compare  
115 one analysis to another, the analyzed volume has to be fixed and comprises the analyzing chamber of the mass spectrometer  
116 and the adjacent volume containing a Zr-Al getter and a charcoal trap. For argon analysis, the trap current is set at  $170\ \mu\text{A}$  with  
117 an electron potential of 60 eV. The acceleration potential is 4.5 kV.

## 118 2.4 Signal corrections

119 Figure 3 shows the signal measured on the H2 cup ( $^{40}\text{Ar}$ ) of a dose of atmospheric argon entering the mass-spectrometer at  $t_0$ .  
120 The gas equilibrium state is achieved 8 seconds after  $t_0$ . An exponential regression is performed on the signal integrated over  
121 a period of 120 seconds to determine the signal at  $t_0$ .

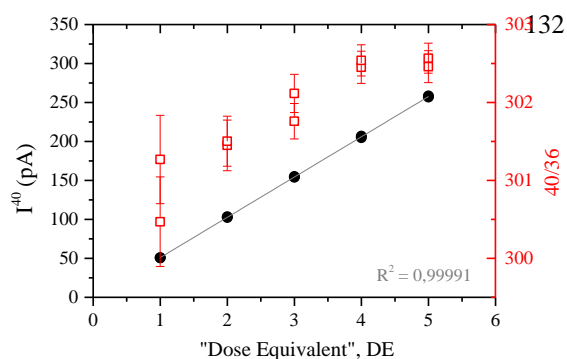


122

123 **Fig. 3 – Intensity measured on the H2 cup ( $^{40}\text{Ar}$ ) of 1DE (atmospheric argon) entering the mass-spectrometer**



124 The sensitivity of the spectrometer depends on the ionization capacities of the source (Loveless and Russell 1969; Werner  
 125 1974; Holst et al., 1999; Rüdenauer 1972), on the gas pressure inside the analyzing chamber (Burnard and Farley, 2000) and  
 126 on the detector type (Turrin et al., 2010). The intensity  $I(^xAr)$  has then to be corrected for the gas pressure effect.  
 127 The pressure dependence is assessed via the analysis of increasing number of calibrated air doses named “Dose-Equivalent”  
 128 (DE) (Charbit et al., 1998b). One DE is determined as the total amount of atmospheric argon contained in one aliquot expanded  
 129 from an air container into the mass-spectrometer (see 0 for details about the air container). The intensity of the isotope 40 and  
 130 the ratio 40/36 measured by the spectrometer from 1 to 5 accumulated DE (replicated) are shown in Fig. 4. Note that the  
 131 depletion of the container for 5 doses is negligible considering isotopic measurement errors.



133

134 **Fig. 4 – Signal of  $^{40}\text{Ar}$  (black dots) and  $^{40}\text{Ar}/^{36}\text{Ar}$  (red square) as a function of the number of accumulated DE sampled from the air**  
 135 **container. The gray line is the linear fit applied to the experimental data. The maximum number of DE has been chosen**  
 136 **considering the saturation value of the cups (400 pA for  $^{40}\text{Ar}$  cup and 40 pA for  $^{38}\text{Ar}$  and  $^{36}\text{Ar}$ ) and the experimental handling**  
 137 **capacities.**

138 According to Fig. 4, the pressure dependence in the mass spectrometer is linear. The relation between the number of DE and  
 139 the  $^{40}\text{Ar}$  signal is given by the following equation:

$$I(^{40}\text{Ar}) = 51\,663 \times \text{DE} - 644 \quad (2)$$

( $R^2 = 0.99991$ )

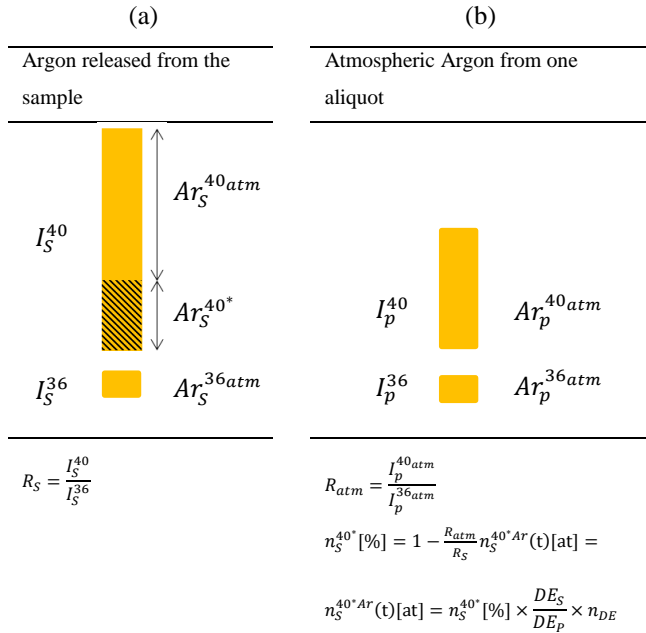
140 The mass discrimination due to the ionization capacities of the electronic source does not significantly depend on the argon  
 141 pressure. Considering uncertainties, the ratio 40/36 of atmospheric argon measured by the mass spectrometer (see Fig. 4) is  
 142 considered to be constant at  $302 \pm 1$ .

## 143 2.5 Analysis procedure

144 The method applied here is based on the unspiked technique described by Cassagnol and Gillot (1982). The argon measurement  
 145 procedure is based on two independent analyses. The first is the measurement of the total  $^{40}\text{Ar}$  released from the sample (Fig.  
 146 5 (a)). The second is the measurement of a calibrated aliquot of atmospheric argon for the quantitative determination of the  
 147 number of  $^{40}\text{Ar}^*$  atoms released from the sample (Fig. 5 (b)). This measurement allows for (1) the determination of the



148 instrumental  $^{40}\text{Ar}/^{36}\text{Ar}$  ratio that we will use to calculate the proportion of  $^{40}\text{Ar}^*$  and (2) the signal calibration, meaning the  
 149 conversion of the signal into a number of atoms.



150 **Fig. 5 – The two-step protocol for measuring radiogenic argon from rock samples (schematic representation derived from Gillot et**  
 151 **al., 2006).  $n_S^{40*} [\text{at}]$  is the number of radiogenic argon from the sample, DE is the number of “Dose-Equivalent” deduced from the**  
 152 **pressure calibration and  $n_{DE}$  is the known amount of  $^{40}\text{Ar}$  in one DE.**

153 The number of  $^{40}\text{Ar}^*$  released from sample per gram is then:

$$n_S^{40*Ar}(t) [\text{at}/g] = n_S^{40*} [\%] \times \frac{DE_S}{DE_P} \times n_{DE} \times \frac{1}{m} \quad (3)$$

154  $n_{DE}$ , the number of atoms of  $^{40}\text{Ar}$  contained in one DE, is calculated from the analysis of standard minerals. Here, this  
 155 calculation relies on the analysis of 7 splits of *HD-B1* (Biotite from the Bergell granodiorite (Italy) (Fuhrmann et al., 1987;  
 156 Schwarz and Trieloff 2007), split 26/7, grain size 200-500 $\mu\text{m}$ ). We have recalculated the amount of  $^{40}\text{Ar}^*$  per gram of HD-B1  
 157 using the value of  $\%K_2O$  determined by SARM following our protocol ( $K_2O = 9.52 \pm 0.01 \%$ , deviation of 0.6% from the  
 158 published value, see Table 3) and the published age of  $t = 24.21 \pm 0.32 \text{ Ma}$ .  $n_{DE}$  was determined with an uncertainty of 0.5%  
 159 achieved from the analysis of 7 *HD-B1* samples. This standard is periodically analyzed (1 over 10 unknown samples) to  
 160 evaluate the deviation of  $n_{DE}$  relative to the time. Also, the pressure calibration is reiterated twice a year because of the depletion  
 161 of the air container after the successive sampling of air aliquots.

162 The final check performed to validate an analysis is the verification of the efficiency of the gas cleanup. A mass scan over  
 163 oxygen pics is performed for each sample using the ARGUS VI mass spectrometer. Validation is made if the oxygen peak  
 164  $m/e=16$  is equal to or lower than that obtained when analyzing an aliquot of air.





165 **2.6 Blank measurements**

166 Blank measurements are periodically performed (1 over 10 samples) to verify that their argon composition is equivalent to the  
 167 atmospheric one (i.e., the absence of radiogenic argon in the system). The protocol for blank measurement is exactly the same  
 168 as for sample analyses. The results of the latest blank measurement are listed in Table 2. <sup>40</sup>Ar blank values are about 37 times  
 169 less than those of 1 DE. The <sup>40</sup>Ar value of the unknowns are usually 10 times higher than the procedural blank. Table 2 also  
 170 presents the electronic blank of the ARGUS VI mass spectrometer (signals on the H2, AX and L2 faraday detectors during  
 171 pumping in the analyzing chamber). Because the composition of this blank is atmospheric, there is no need to deduce it from  
 172 the signal of the sample. This induces that our measurement of the proportion of radiogenic argon ( $n_s^{40*}$  [%]) is reduced. Our  
 173 measurements so far lead to an underestimation from 1 to 10% of the proportion of the radiogenic argon initially contained in  
 174 the sample. The underestimation of this value depends on the <sup>40</sup>Ar intensity ratio between the blank and the sample.

175 **Table 2 – Intensity of line blanks compared to one DE**

	I <sup>40</sup> (fA)	I <sup>38</sup> (fA)	I <sup>36</sup> (fA)	40/36	40/38
Electronic Blank	7.3±0.4	-0.2±0.2	-1.0±0.2	-	-
Furnace Blank	1 358.8±3.1	0.8±0.2	4.7±0.3	291±17	1 793±585
1 DE	50 682±5	31.9±0.2	168.7±0.3	301.3±0.6	1 597±13

176 **2.7 Reference materials**

177 To our knowledge, no clay material is used as a reference material for K-Ar dating. Three micas (or related) of different ages  
 178 were chosen instead to validate the protocol for measuring potassium and argon:

- 179 - *GL-O*, the glauconite of Odin from the Cauville cliff (France), reference material (Odin, 1982; Boulesteix et al.,  
 180 2020);
- 181 - *BMus2*, a muscovite from the Bärhalde granite in the Black Forrest (Germany) (Rittmann, 1984), used as an in-house  
 182 standard by (Schwarz and Trieloff, 2007);
- 183 - *PANXVII-3*: large muscovite selvage of quartz vein from Panasqueira (Portugal), in-house reference material dated  
 184 by K-Ar (Snee et al., 1988) and more recently by Ar/Ar (Carocci et al., 2020).

185 Table 3 compares the ages obtained at GeoRessources to those from the literature of the three micas. The deviation from the  
 186 literature of ages is less than 0.6%, which is lower than the uncertainty on the individual ages. These results validate the  
 187 protocol used to measure potassium and radiogenic argon at GeoRessources.



188 **Table 3 – Comparison of potassium content and ages of reference materials from the literature to those obtained at the SARM**  
 189 **(CRPG) and GeoResources**

	%K <sub>2</sub> O Lit.	%K <sub>2</sub> O SARM	Age (Ma) Lit.	Age (Ma) GeoR
HD-B1 (Fuhrmann et al., 1987; Schwarz and Trieloff, 2007)	9.58 ± 0.02	9.52 ± 0.14	24.21 ± 0.32	-
B/Mus2 (Schwarz and Trieloff, 2007; Rittmann, 1984)	10.20	10.13 ± 0.15	328.5 ± 1.1	324.5 ± 3.2
GL-O (Odin, 1982)	6.56 ± 0.10	6.56 ± 0.10	95.0 ± 1.0	95.3 ± 1.0
PANXVII-3 (Snee et al., 1988; Carocci et al., 2020)	[9.91:10.67] ± 0.15	10.19 ± 0.15	296.3 ± 0.6	295.3 ± 1.5

### 190 3 Characterizing and Dating Illite

191 Clay fractions often contain a mixture of various illites polytypes (Bailey, 1966), from possibly different origins (detrital and  
 192 authigenic) and generations (Clauer, 2013). Common illite polytypes are 1Md, 1M and 2M<sub>1</sub> (Reynolds and Thomson, 1993).  
 193 In sedimentary units, the 2M<sub>1</sub> illite polytype is considered as a detrital component due to its inert behavior in anchizonal to  
 194 epizonal conditions (Bailey, 1966; Środoń and Eberl, 1984). It generally forms thicker platy crystallites shaped with irregular  
 195 edges because they are subjected to some dissolution and erosional processes since crystallization (Clauer, 2013). The 1Md  
 196 and 1M illite polytypes are considered as authigenic products formed under diagenetic to anchi-metamorphic conditions  
 197 (Grathoff and Moore, 1996). They generally are platy to fibrous or lath-shaped (Peltz et al., 2022).  
 198 The separation of illite polytypes of different origin and generations is commonly attempted by separating illites by their  
 199 particle size. XRD analyses and SEM observations are then performed on each size fraction with the main objective of relating  
 200 mineralogical, crystallographic and morphological characteristics of the various illite populations to their crystallization ages.

#### 201 3.1 Separation

202 A large amount of clay material is needed to perform XRD and K-Ar dating (see section 2.1). The following procedure is  
 203 adapted from conventional separation techniques, enabling the production of large amounts of datable clays.  
 204 The sample material is first gently crushed using a mortar or different grinding machines depending on the stiffness of the  
 205 sample. The so-crushed sample is added to deionized water for disaggregation in an ultrasonic bath for approximately 30 min.  
 206 First, the coarse fractions (typically <2µm, 2-5 µm and 5-10 µm) are separated using gravity sedimentation based on the  
 207 Stokes' law. For this, the disaggregated sample is poured into 2L cylinders placed in a thermo-statically controlled water tank.  
 208 The GeoResources laboratory owns two in-house designed water tanks that can carry six 2L cylinders each. Both are fitted  
 209 with a tube system that connects the cylinders to a water pump, so to minimize the vibrations during sampling. To increase the  
 210 efficiency of the separations and the yield of the suspensions (especially <2 µm), sampling of the same size fraction is  
 211 performed several times on (1) the remaining solution and (2) the sampled solution. The <2 µm fraction is used to separate  
 212 smaller fractions down to at least <0.1 µm, using the centrifuge Beckman-Coulter Avanti J-26S XP fitted with the JCF-Z



213 continuous flow rotor coupled to a calibrated peristaltic pump. This system allows for separating fractions directly during  
214 centrifugation. The time required for the procedure depends only on the volume of the solution to be separated. For example,  
215 the separation of 4L of solution generally lasts around 20 minutes, that is much faster than the several days needed with a  
216 classical separation technique (Poppe et al., 2001).

217 Fractions of 1-2  $\mu\text{m}$ , 0.5-1  $\mu\text{m}$  and  $< 0.5 \mu\text{m}$  were separated using the following parameters derived from (Viola et al., 2018):  
218 (3000 RPM; 350mL/min) for the  $< 1 \mu\text{m}$ , (1270 RPM; 250mL/min) for the  $< 0.5 \mu\text{m}$ , (6000 RPM; 230mL/min) for the  $< 0.2$   
219  $\mu\text{m}$  and (10 000 RPM; 160mL/min) for the  $< 0.1 \mu\text{m}$ . Supernatants were then collected by centrifugation using the same  
220 centrifuge fitted with the JA-10 rotor with the following parameters: (6000 RPM; 10 min) for 1-2  $\mu\text{m}$ , (7000 RPM; 10 min)  
221 for 0.5-1  $\mu\text{m}$  and (9000 RPM; 20 min) for all fractions below 0.5  $\mu\text{m}$ . The remaining excess of water is removed by air drying  
222 for a few days.

223 The efficiency of this separation protocol was monitored using a laser particle sizer and SEM observations. An example of the  
224 particle size proportion estimated in each separated fraction is shown in 0. As expected, a clear reduction of particle size is  
225 observed in the finer fraction.

226 Coupling the large capacities of the Stokes' benches to the centrifuge fitted with the continuous flow rotor increases our ability  
227 to collect large amounts of fractions, especially for the finest particles. For example, 200mg of the  $< 0.5 \mu\text{m}$  fraction was  
228 isolated from a 55g sample of fault gouge. Thus, this device and its associated separation protocol provide sufficient material  
229 for carrying out mineralogical characterization by XRD and K-Ar geochronology.

### 230 **3.2 Structural and mineralogical characterization**

231 SEM observations are performed on a TESCAN VEGA III equipped with an energy dispersive spectrometer (EDS) at the  
232 SCMEM (Service Commun de Microscopies Electroniques et de Microanalyses) at GeoRessources. First, thin sections, chips  
233 or polished sections of the whole rock are observed to obtain some structural and textural information. Secondly, the separated  
234 fractions are observed to (1) verify the size of the particles and (2) identify the morphology in each fraction. In the example  
235 given in 0, particles of the coarse fractions are platy and hairy in the finer fractions. One can assume at this stage that the  
236 sample contains two different polytypes of illite, possibly formed during successive geological events.

237 The different clays minerals are characterized by XRD using the Bruker D2 phaser equipped with a copper tube (35 kV, 40  
238 mA). First, oriented mounts of the  $< 2\mu\text{m}$  fractions are prepared following the methods of Moore and Reynolds (1997) and  
239 scanned over a range of  $2$  to  $40^\circ 2\theta$  with a step size of  $0.02^\circ 2\theta$  and a 1 second count time per step. The identification of clay  
240 minerals is performed by comparing the diffractograms obtained under air-dry (AD), ethylene-glycol solvation (EG) and  
241 heating at  $490^\circ\text{C}$  (H). The comparison between (1) the AD and EG XRD diffractograms allows for the identification of the  
242 illite/smectite mixed-layer and (2) the AD and H for kaolinite identification (Holtzapffel, 1986). The values of the illite  
243 crystallinity are expressed by the Kübler index (KI) (Klüber, 1966). Randomly oriented powder are also mounted using a Si-  
244 low background sample holder with a 0.5 mm sample cavity. The sample holder is filled by the side as recommended by  
245 Grathoff and Moore (1996). The orientation randomness is checked by the ratio of the (002)/(020) illite peaks, which should



246 be low for non-oriented samples. This preparation is scanned over a range of 16 to 38° 2 $\theta$  with a step size of 0.01 °2 $\theta$  and a 3-  
247 second count time per step.

248 The peaks corresponding to the polytypes of illite (i.e. 2M1, 1M and 1Md) are identified using the approach proposed by  
249 Grathoff and Moore (1996). The proportion of the 2M1 and 1M polytypes are determined by obtaining the ratio of the area (or  
250 the height) of each polytype peaks to the area of the peak at 2.58Å, which is common to all illite polytypes. If the sum of 2M1  
251 and 1M is smaller than 100%, the difference could be attributed either to the presence of the 1Md polytype, or to a slight  
252 preferential orientation. The obtained percentages of polytypes are cross-checked by comparing the experimental XRD  
253 diagram with the XRD patterns modeled by the Wildfire© software. If kaolinite is present in the clay fraction, the randomly  
254 oriented powder mount is heated to 550°C to prevent kaolinite peak from interfering with the hkl peak at 2.56 Å, and is  
255 rescanned.

### 256 3.3 Dating interpretation

#### 257 3.3.1 Method

258 Each separated fraction is dated by the K-Ar method using the procedure described in the 2.5 section. As each fraction contains  
259 a mixture of illite polytypes, individual ages have little geological meaning. As mentioned in Hueck et al., (2022), two  
260 strategies can be applied to decipher geochronological information from the set of K-Ar ages.

261 The first is the limit age interpretation, generally applied when polytype quantification is not available. The date obtained on  
262 the finest fraction that most likely contains authigenic material, represents the maximum age of the illite authigenesis.  
263 Conversely, the date obtained on the coarsest fraction, most likely containing inherited material, represents the minimum age  
264 of the oldest illitization (detrital illite in the case of sedimentary units).

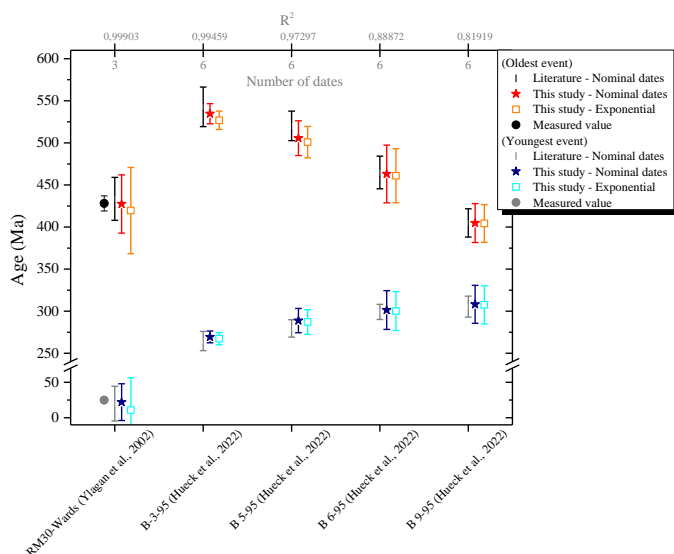
265 The second approach is the Illite-Age-Analysis (IAA) developed by Pevear (1992), in which end-member ages are determined  
266 by extrapolating the set of individual dates. Assuming that the sample contains a mixture of two illite populations, the end-  
267 member dates reflect the ages of the oldest and youngest geological events. The proportion of the two populations of illite  
268 must be determined so to evaluate the dates at 0% and 100% of one population (100% and 0% of the other). The extrapolation  
269 of end-member dates is generally performed using an error-weighted linear regression based on the least-square method applied  
270 to the set of individual dates (Van der Pluijm et al., 2001). The 90% confidence intervals are also calculated to define the error  
271 on the extrapolated ages. To consider the non-linearity of the age equation, some authors prefer to fit the data expressed as  $e^{\lambda t}$   
272 - 1 (Van der Pluijm et al., 2001; Ylagan et al., 2000; Haines and Van der Pluijm, 2023; Song and Sim, 2021), since it is a linear  
273 function with the ratio of radiogenic argon to potassium.

#### 274 3.3.2 Application

275 To validate the IAA method applied at GeoRessources, two sets of dates published in the literature were used: (1) the set of  
276 dates of synthetic mixtures of two pure illite fractions, 2M1 (Wards – 428.0 ± 9.0 Ma) and 1M (RM-30 – 24.8 ± 0.6 Ma)



277 prepared by Ylagan et al. (2002) and (2) the set of dates of metapelites from the Rhenish massif from the recent study of Hueck  
 278 et al. (2022). The ages obtained by fitting either the set of nominal dates or the exponential terms are presented in Fig. 6 along  
 279 with literature data (measured and extrapolated ages). R-square is also shown in the figure as well as the number of dates  
 280 available for the fit.



281  
 282 **Fig. 6 – Comparison of extrapolated ages obtained by IAA between literature data and this study. The ages of RM-30 and Wards**  
 283 **samples measured by Ylagan et al. (2002) are also shown.**

284 Considering the uncertainties, one can reasonably state that the extrapolated ages calculated in this work are similar to those  
 285 from the literature. Most notably, this present work successfully outputs the ages of the two pure illite fractions of Ylagan et  
 286 al. (2002). Also, fitting the data using the exponential term does not significantly change the ages, as expected according to  
 287 Ylagan et al. (2000).

288 In this work, fits are weighted by instrumental error ( $w_i=1/\sigma^2$ ,  $\sigma$  being the individual date error). Consequently, the uncertainties  
 289 will be reduced when fitting precise dates (sample B-3-95). Larger uncertainties than the published ones can be explained  
 290 either by a limited set of dates, by high individual uncertainties on the dates (see samples B-6-95 and B-9-95, Hueck et al.,  
 291 2022) or by the difference in the level of the confidence interval, 90% in this work and that of Ylagan and 68% for Hueck’s  
 292 study. Thus, to obtain valuable extrapolated ages, we recommend the following considerations:

- 293 - The fit should be weighted by the instrumental error;
- 294 - The level of confidence should be 90%;
- 295 - The data set should contain at least 4 dates (i.e. 4 separated fractions) and ideally, they will be distributed between 0  
 296 to 100% of one polytype.

297 Finally, it is essential to remember that the IAA method assumes that only two different polytypes are present in the illitic  
 298 mixture. Also, the 2M1 illite must be either inherited or authigenic, and the 1M/1Md illite must be authigenetic (Hueck et al.,



299 2022). For the successful application of the IAA, those assumptions must be validated by complementary chemical,  
300 morphological and crystallographic data. More than two populations of illite might be detected either by the complementary  
301 analyses, or by the difficulty to obtain a proper linear regression on the set of dates obtained on the separated fractions (if each  
302 population relates to distinct geological events considering the precision of K-Ar dating).

#### 303 **4 Conclusion**

304 Deciphering the origin of illites in a mixture of clays relies on (1) a proper separation of the clay material (at least 4  
305 granulometric fractions) containing various proportions of illite material (ideally distributed between 0 to 100%), (2) a precise  
306 characterization of the mineralogy and the morphology by SEM, EDS and XRD of each size fraction, (3) the determination of  
307 a precise age of each size fraction by the K-Ar method and (4) the interpretation of the ages obtained by the IAA method  
308 enabling the identification of two geological events. Each of these four critical points was addressed in this paper in order to  
309 validate the method and protocols developed on the novel platforms of GeoRessources, which include the clay separation  
310 laboratory for large quantities and the K-Ar method.

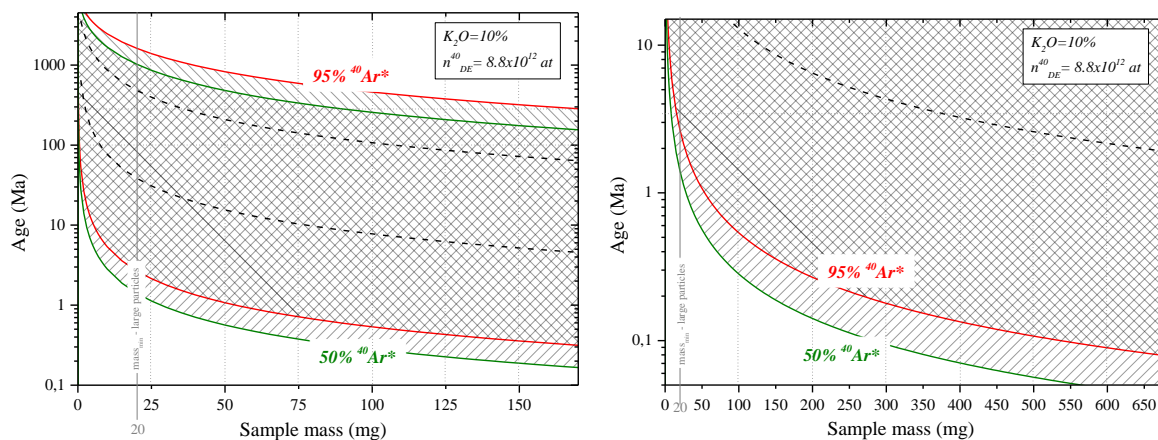
311 This integrated method offers a powerful tool to provide constraints of various physical and chemical processes occurring at  
312 the micro- and nanoscale, improving our understanding of the evolution of the Earth system.

#### 313 **Appendix**

##### 314 **A Mass ranges accepted in the desorption line depending on expected ages**

315 Sample masses are measured on a Mettler XSU105DU with a resolution of 0.00001g in the 0-41 g range, which is calibrated  
316 every year by a certified company. The absolute error on the mass is set at 0.02mg.

317 The following plots illustrate the sample mass range accepted in the desorption line depending on age. Simulations are  
318 performed considering (1) the range of pressure accepted in the mass spectrometer and (2) the K<sub>2</sub>O proportion of 10% (mica).  
319 For example, the mass of a large particle-sized sample with an expected age of about 500 Ma should range between 20 mg and  
320 50 mg. For a sample of an expected age of about 1 Ma, the mass minimum should be 50 mg.



321

322 **Fig. A1 – Ranges of mass accepted in the desorption line at GeoResources depending on the expected age of the sample. Simulations**  
 323 **are performed for 50 (green) and 95% (red) of radiogenic argon. The dense pattern represents the area of interest.**

324 This wide range of masses and ages accepted in the desorption line is possible using three protocols implying additional gas  
 325 expansion steps (when the argon pressure is high). The black dotted lines separate the areas of application of each protocol.

326 **B Comparison of clay weight loss during annealing and vacuum pumping**

327 This experiment was carried out on aliquots of < 2 μm clay particles. Aliquots (a to d) have been weighed before and after  
 328 annealing at 105°C under air or vacuum pumping. Storage under vacuum or in the furnace lasts from 1 to 25 days. The loss of  
 329 mass of the samples is presented in the Table 4. Independently of the mass of the aliquots, the furnace (A or B) and the storage  
 330 duration, the weight losses after 105°C annealing and after vacuum pumping are close: around 0.76% under annealing and  
 331 0.92% under vacuum.

332 **Table B1 – Comparison of clay weight loss during annealing and vacuum pumping**

Sample Name	Mass	Treatment	Days	weight-loss (%)
WC448[<2]a	> 1g	Annealing at 105°C Furnace A	1	0.76
			2	0.75
			3	0.73
			7	0.65
			8	0.70
			13	0.82
WC448[<2]b	0.341 g	Annealing at 105°C Furnace B	1	0.76
WC448[<2]c	22.95 mg	Turbo-molecular pumping	1	0.92
			25	0.78
WC448[<2]d	51.01 mg	Turbo-molecular pumping	1	0.92
			25	0.96

333 A similar experiment was performed on GL-O (Odin’s standard glauconite) (Odin 1982). The weight loss after a few days of  
 334 vacuum pumping lies between 2.51 and 3.14% (8 samples studied), in agreement with Zimmermann and Odin (1979) who



335 found a weight loss of about 3% by dehydration of the glauconite. The weight loss measured after vacuum storage of the  
336 samples is then due to the pumping of adsorbed gas and dehydration of samples.

337 Besides uncertainties, the slightly higher weight-loss values found on the clay aliquots stored under vacuum could be explained  
338 by the dehydration of clays that might be more efficient under vacuum than in a furnace at 105°C.

### 339 **C Filling the calibrated air container**

340 The calibration sector consists of a dried air container connected to an expansion valve. The amount of argon in the expansion  
341 valve after  $i$  individual dose taken from the container ( $n_i$ ) is given by:

$$\begin{cases} n_i = n_0 \times \left( \frac{1}{1 + \frac{v}{V_b}} \right)^i \\ n_0 = n_B \times \left( \frac{v}{V_b} \right) \end{cases} \quad (4)$$

342 Where  $n_0$  is the amount of argon in the first dose,  $v$  is the volume of the expansion valve (approximated),  $V_b$  is the volume of  
343 the container and  $n_B$  is the initial amount of argon in the container (after filling).

344 Before filling the air container, the amount of argon expected in the expansion valve has been calculated so as to obtain a DE  
345 signal comparable to that of the samples. According to eq.(4), the amount of argon required in the expansion valve determines  
346 the amount of air to introduce in the container. Thus, the calibrated container has been specifically designed for the ARGUS  
347 VI mass spectrometer measurements tuned with specific source parameters.

348 The desired pressure of air in the container is calculated as follows:

$$P_b(\text{air}) \approx \frac{R \times T}{\%(\text{Ar}) \times \%(^{40}\text{Ar}) \times N_A} \times \left( \frac{1}{v} + \frac{1}{V_b} \right) \times \frac{I_{\text{aliquot}}(^{40}\text{Ar})}{S} \quad (5)$$

349 Where  $I_{\text{aliquot}}(^{40}\text{Ar})$  (fA) is the intensity measured by the mass spectrometer of  $^{40}\text{Ar}$  from the air aliquot,  $S$  (pA/at) is the  
350 sensitivity of the mass spectrometer,  $\%(\text{Ar})$  is the proportion of argon in air and  $\%(^{40}\text{Ar})$  is the proportion of the isotope 40 of  
351 argon.

352 To fill the container with this desired air pressure, a protocol of successive expansions and pumping was established using a  
353 set of two volumes  $V_0$  and  $V_x$ . Following this protocol, the air pressure in the container is:

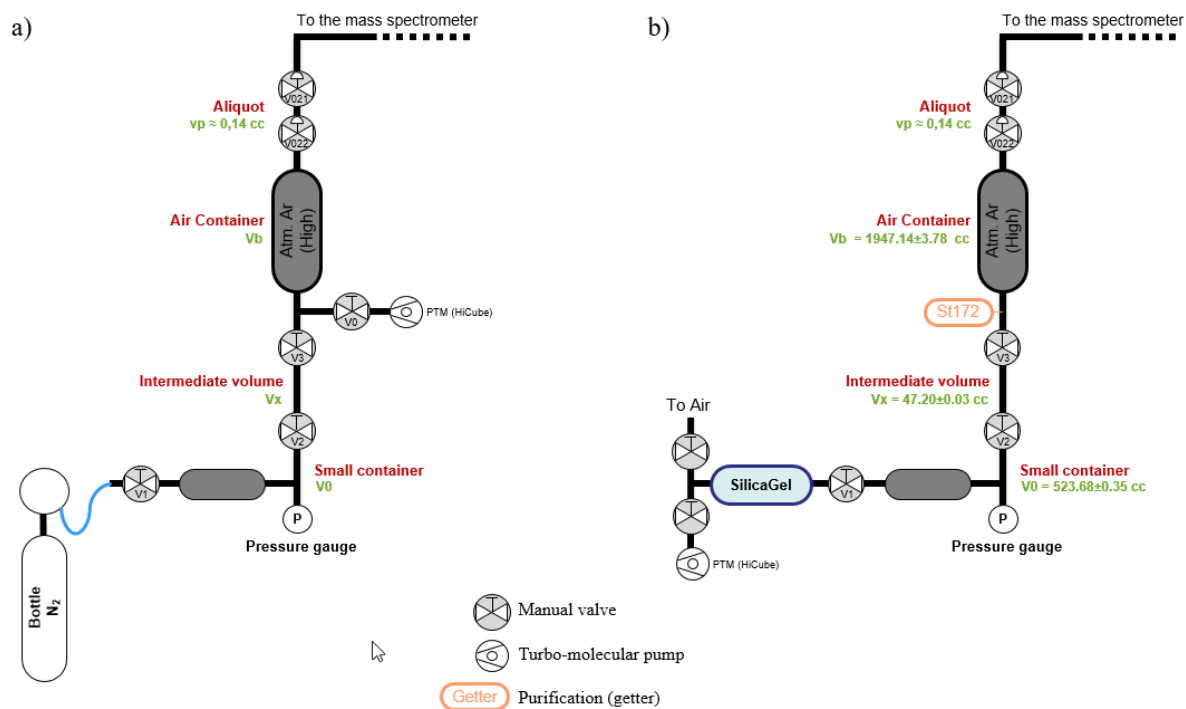




$$P_b = P_0 \times \frac{1}{\left(\frac{V_0}{V_x} + 1\right)^2} \times \frac{1}{\left(\frac{V_b}{V_x} + 1\right)} \times \frac{1}{\left(\frac{V_0 + V_x}{V_b} + 1\right)^2} \quad (6)$$

$$P_b = 9.84 \pm 0.04 \text{ Pa}$$

354 Note that this pressure is too low to be measured by the manometers available at the laboratory. The two volumes  $V_0$  and  $V_x$   
 355 were designed with the objective of minimizing the number of expansion and so, minimizing the error on the container  
 356 pressure. Volumetric measurements yield values of  $523.68 \pm 0.35$  cc for  $V_0$  and  $47.20 \pm 0.03$  cc for  $V_x$ . The volume of the  
 357 container was determined by pressure measurement of nitrogen expanded from  $V_0 + V_x$  to  $V_b$  (see Fig. C1 Fig. (a) for a scheme  
 358 of the experimental setup). Successive measurements allow for a precise determination of  $V_b$  of  $1947.1 \pm 3.8$  cc. The scheme  
 359 of the experimental setup for filling the air container is presented in C1(b). Note that the replacement of the valve  $V_0$  by the  
 360 SAES getter St172 does not significantly change the volume of the container (the volume difference is in the uncertainty).  
 361



362

363 Fig. C1 – Schematic representation of the setup designed to a) measure the volume of the container and b) fill it with dried air.

364

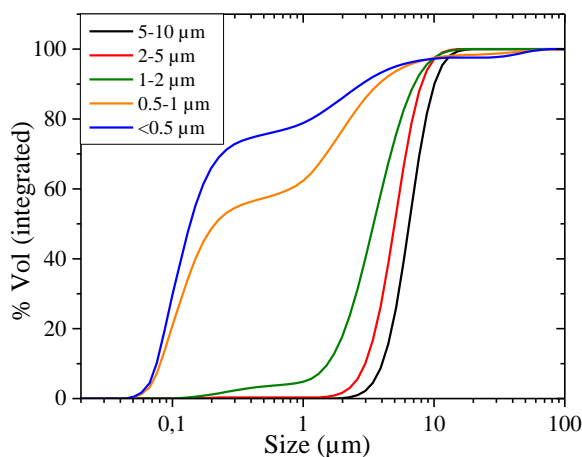
365

366



367 **D Laser diffraction analyses and SEM observations of the separated fractions**

368 Granulometric analyses are performed at Chrono-Environnement (Besançon, France) on the LS230 Beckman Coulter laser  
369 particle size analyzer. An example of the particle size proportion estimated in each separated fraction is shown in Fig. D1. In  
370 the tested samples, only large clay particles were present, from 10  $\mu\text{m}$  down to  $< 0.5 \mu\text{m}$  (an insignificant amount of clay were  
371 present in the  $< 0.2 \mu\text{m}$  fraction). The proportion of fine particles increases in the finer fractions to 75% of particles below 0.5  
372  $\mu\text{m}$  in the so-called  $< 0.5 \mu\text{m}$  fraction. However, in the so-called 2-5  $\mu\text{m}$  fraction, 90% is above 2  $\mu\text{m}$  with 50% above 5  $\mu\text{m}$ .

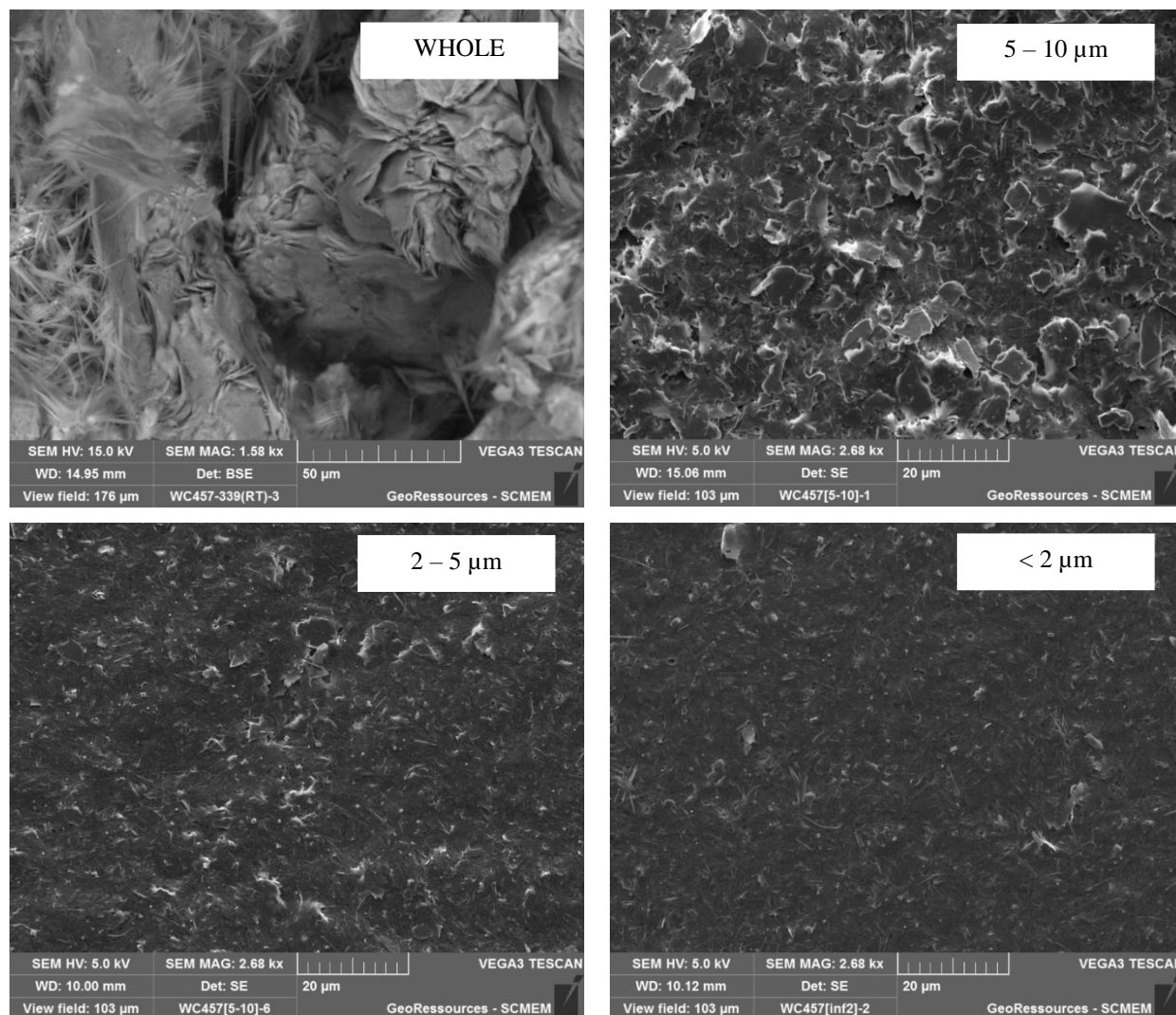


373

374 **Fig. D1 –Particle size distribution in each separated fraction calculated by the Mie’s theory on laser diffraction data.**

375 The results of the laser diffraction are based on calculations using the Mie’s theory hypothesis (Eremin 2005), which considers  
376 spherical particles, isotropic and homogeneously distributed. Since clay minerals are platy to hairy shaped, the calculation of  
377 the particle size is naturally biased. Granulometric analysis based on laser diffraction is then not used for clay size  
378 measurements but rather for controlling the separation step.

379 SEM observations were performed on the whole rock of a fault gouge sample and on separated 5-10  $\mu\text{m}$ , 2-5  $\mu\text{m}$  and  $< 2 \mu\text{m}$   
380 fractions. The separated fractions were observed after dropping the fractions diluted with ethanol on an SEM pad. Two  
381 morphologies can be identified on the whole rock: platy and hairy illites. The platy illite is dominant in the 5-10  $\mu\text{m}$  and the  
382 hairy is dominant in the finer fraction. The 2-5  $\mu\text{m}$  seems to contain the two morphologies, including platy illite with a smaller  
383 size than in the 5-10  $\mu\text{m}$  fraction.



384 Fig. D2 – SEM observations of a fault gouge sample, whole rock and separated fractions 5-10μm, 2-5μm and 2μm. All fractions were  
385 observed at the same magnitude except the whole rock.

### 386 Competing interests

387 The authors declare that they have no conflict of interest.

### 388 Author contribution

389 **Marie Gerardin**: Project administration, Data curation, Formal analysis, Investigation, Methodology, Validation,  
390 Visualization, Writing – original draft preparation; **Gaétan Milesi**: Investigation, Methodology, Writing – original draft  
391 preparation; **Julien Mercadier**: Funding acquisition, Resources, Supervision; **Michel Cathelineau**: Funding acquisition,



392 Conceptualization, Resources, Supervision; **Danièle Bartier**: Formal analysis, Investigation, Methodology, Writing – original  
393 draft preparation.

#### 394 **Acknowledgment**

395 The argon desorption setup was mainly funded by the LabEx RESSOURCES21 by the University of Lorraine and from Carnot  
396 and ERAMIN “MOSTMEG” funding programs. We want to acknowledge the important work of P. Robert (University of  
397 Lorraine) on his initial contribution on the development of the argon desorption line. We thank W. Schwarz (University of  
398 Heidelberg) for the discussions and the HD-B1 and B/Mus2 reference materials. We thank G. Viola (University of Bologna)  
399 and R. Van der Lelij (NGU, Norway) for discussing clay mineral separation, notably using the centrifuge. We thank Marguerite  
400 Perrey (Chrono-environnement, Besançon) for the laser diffraction analyses and the discussion about the size calculations. We  
401 thank N. Clauer (University of Strasbourg) for discussion about clay minerals dating by the K-Ar method and for reviewing  
402 this work. Many thanks to H. Guillou (LSCE, CEA Saclay) for the donation of his induction furnace and small Ti ceramic  
403 furnaces, and for all the discussion about K-Ar dating. Finally, a special thank is addressed to J-C. Lefèvre (GEOPS, Université  
404 Paris-Saclay) for the numerous discussions and meetings, and his significant technical help on the development of the argon  
405 desorption line.

#### 406 **References**

- 407 Akker, I. V., Berger, A., Zwingmann, H., Todd, A., Schrank, C. E., Jones, M. W. M., Kewish, C. M., Schmid, T. C., and  
408 Herwegh, M.: Structural and chemical resetting processes in white mica and their effect on K-Ar data during low temperature  
409 metamorphism, *Tectonophysics*, 800, 228708, <https://doi.org/10.1016/j.tecto.2020.228708>, 2021.
- 410 Aldrich, L. T. and Nier, A. O.: Argon 40 in Potassium Minerals, *Phys. Rev.*, 74, 876–877,  
411 <https://doi.org/10.1103/PhysRev.74.876>, 1948.
- 412 Bailey, S. W.: The Status of Clay Mineral Structures, *Clays Clay Miner.*, 14, 1–23,  
413 <https://doi.org/10.1346/CCMN.1966.0140101>, 1966.
- 414 Boulesteix, T., Solé, J., Pi, T., and Cathelineau, M.: Reappraisal of the GL-O Reference Material for K-Ar Dating: New Insight  
415 from Microanalysis, Single-Grain and Milligram Ar Measurements, *Geostand. Geoanalytical Res.*, n/a,  
416 <https://doi.org/10.1111/ggr.12306>, 2020.
- 417 Brockamp, O. and Clauer, N.: Hydrothermal and unexpected diagenetic alteration in Permian shales of the Lodève epigenetic  
418 U-deposit of southern France, traced by K–Ar illite and K-feldspar dating, *Chem. Geol.*, 357, 18–28,  
419 <https://doi.org/10.1016/j.chemgeo.2013.08.009>, 2013.
- 420 Burnard, P. G. and Farley, K. A.: Calibration of pressure-dependent sensitivity and discrimination in Nier-type noble gas ion  
421 sources: TECHNICAL BRIEF, *Geochem. Geophys. Geosystems*, 1, n/a-n/a, <https://doi.org/10.1029/2000GC000038>, 2000.



- 422 Carocci, E., Marignac, C., Cathelineau, M., Truche, L., Poujol, M., Boiron, M.-C., and Pinto, F.: Incipient Wolframite  
423 Deposition at Panasqueira (Portugal): W Rutile and Tourmaline Compositions as Proxies for the Early Fluid Composition,  
424 *Econ. Geol.*, <https://doi.org/10.5382/econgeo.4783>, 2020.
- 425 Cassagnol, C. and Gillot, P.-Y.: Range and Effectiveness fo Unspiked Potassium-Argon Dating: Experimental Groundwork  
426 and Applications, John Wiley N. Y., 1982.
- 427 Cattani, F., Gillot, P.-Y., Quidelleur, X., Hildenbrand, A., Lefèvre, J.-C., Boukari, C., and Courtade, F.: In-situ K-Ar dating  
428 on Mars based on UV-Laser ablation coupled with a LIBS-QMS system: Development, calibration and application of the  
429 KArMars instrument, *Chem. Geol.*, 506, 1–16, <https://doi.org/10.1016/j.chemgeo.2018.12.010>, 2019.
- 430 Charbit, S., Guillou, H., and Turpin, L.: Cross calibration of K–Ar standard minerals using an unspiked Ar measurement  
431 technique, *Chem. Geol.*, 150, 147–159, 1998a.
- 432 Charbit, S., Guillou, H., and Turpin, L.: Cross calibration of K–Ar standard minerals using an unspiked Ar measurement  
433 technique, *Chem. Geol.*, 150, 147–159, 1998b.
- 434 Clauer, N.: The K-Ar and  $^{40}\text{Ar}/^{39}\text{Ar}$  methods revisited for dating fine-grained K-bearing clay minerals, *Chem. Geol.*, 354,  
435 163–185, <https://doi.org/10.1016/j.chemgeo.2013.05.030>, 2013.
- 436 Clauer, N.: How Can Technical Aspects Help Improving K-Ar Isotopic Data of Illite-Rich Clay Materials into Meaningful  
437 Ages? The Case of the Dominique Peter Uranium Deposit (Saskatchewan, Canada), *Geosciences*, 10, 285,  
438 <https://doi.org/10.3390/geosciences10080285>, 2020a.
- 439 Clauer, N.: The post-Variscan tectonic-thermal activity in the southeastern metalliferous province of the French Massif Central  
440 revisited with K-Ar ages of illite, *Ore Geol. Rev.*, 117, 103300, <https://doi.org/10.1016/j.oregeorev.2019.103300>, 2020b.
- 441 Clauer, N., Zwingmann, H., Liewig, N., and Wendling, R.: Comparative  $^{40}\text{Ar}/^{39}\text{Ar}$  and K–Ar dating of illite-type clay  
442 minerals: A tentative explanation for age identities and differences, *Earth-Sci. Rev.*, 115, 76–96,  
443 <https://doi.org/10.1016/j.earscirev.2012.07.003>, 2012.
- 444 Dalrymple, G. B. and Lanphere, M. A.: Potassium-argon dating: principles, techniques and applications to geochronology,  
445 Freeman, San Francisco., 1969.
- 446 Fuhrmann, U., Lippolt, H. J., and Hess, J. C.: Examination of some proposed K-Ar standards:  $^{40}\text{Ar}/^{39}\text{Ar}$  analyses and  
447 conventional K-Ar data, *Chem. Geol. Isot. Geosci. Sect.*, 66, 41–51, [https://doi.org/10.1016/0168-9622\(87\)90027-3](https://doi.org/10.1016/0168-9622(87)90027-3), 1987.
- 448 Garner, E. L., Murphy, T. J., Gramlich, J. W., Paulsen, P. J., and Barnes, I. L.: Absolute isotopic abundance ratios and the  
449 atomic weight of a reference sample of potassium, *J. Res. Natl. Bur. Stand. Sect. Phys. Chem.*, 79A, 713,  
450 <https://doi.org/10.6028/jres.079A.028>, 1975.
- 451 Gillot and Cornette: The Cassagnol technique for potassium—Argon dating, precision and accuracy: Examples from the Late  
452 Pleistocene to Recent volcanics from southern Italy, *Chem. Geol. Isot. Geosci. Sect.*, 59, 205–222, 1986.
- 453 Gillot, P.-Y., Hildenbrand, A., Lefevre, J.-C., and Albore-Livadie C.: The K/Ar dating method : principle, analytical  
454 techniques, and application to Holocene volcanic eruptions in Southern Italy, *Acta Vulcanol.*, 18, 55–66, 2006.
- 455 Grathoff, G. H. and Moore, D. M.: Illite Polytype Quantification using WILDFIRE© Calculated X-Ray Diffraction Patterns,  
456 *Clays Clay Miner.*, 44, 835–842, <https://doi.org/10.1346/CCMN.1996.0440615>, 1996.



- 457 Grau Malonda, A. and Grau Carles, A.: Half-life determination of  $^{40}\text{K}$  by LSC, *Appl. Radiat. Isot.*, 56, 153–156,  
458 [https://doi.org/10.1016/S0969-8043\(01\)00181-6](https://doi.org/10.1016/S0969-8043(01)00181-6), 2002.
- 459 Guillou, H., Nomade, S., and Scao, V.: The  $^{40}\text{K}/^{40}\text{Ar}$  and  $^{40}\text{Ar}/^{39}\text{Ar}$  Methods, in: *Paleoclimatology*, edited by: Ramstein,  
460 G., Landais, A., Bouttes, N., Sepulchre, P., and Govin, A., Springer International Publishing, Cham, 73–87,  
461 [https://doi.org/10.1007/978-3-030-24982-3\\_5](https://doi.org/10.1007/978-3-030-24982-3_5), 2021.
- 462 Haines, S. H. and van der Pluijm, B. A.: Fault Gouge Dating in the Spanish Pyrenees: Fault Ages, Thrust Propagation  
463 Sequence, Wall-Rock Provenance, and Thermal Constraints, *Tectonics*, 42, e2022TC007251,  
464 <https://doi.org/10.1029/2022TC007251>, 2023.
- 465 Holst, B., Buckland, J. R., and Allison, W.: Spatial mapping in the electron-impact ion-source of a residual gas analyser,  
466 *Vacuum*, 53, 207–210, [https://doi.org/10.1016/S0042-207X\(98\)00388-1](https://doi.org/10.1016/S0042-207X(98)00388-1), 1999.
- 467 Holtzapffel, T.: *Minéraux argileux lattes : les smectites du domaine atlantique*, Université d'Angers, 1986.
- 468 Hueck, M., Wemmer, K., Ksienzyk, A. K., Kuehn, R., and Vogel, N.: Potential, premises, and pitfalls of interpreting illite  
469 argon dates - A case study from the German Variscides, *Earth-Sci. Rev.*, 232, 104133,  
470 <https://doi.org/10.1016/j.earscirev.2022.104133>, 2022.
- 471 Klüber, B.: La cristallinité de l'illite et les zones tout a fait supérieures du métamorphisme., *Étages Tecton. Colloq. Neuchâtel*  
472 1966 Baconnière Neuchâtel, 105–121, 1966.
- 473 Kralik, M., Klima, K., and Riedmüller, G.: Dating fault gouges, *Nature*, 327, 315–317, <https://doi.org/10.1038/327315a0>,  
474 1987.
- 475 Lee, J.-Y., Marti, K., Severinghaus, J. P., Kawamura, K., Yoo, H.-S., Lee, J. B., and Kim, J. S.: A redetermination of the  
476 isotopic abundances of atmospheric Ar, *Geochim. Cosmochim. Acta*, 70, 4507–4512,  
477 <https://doi.org/10.1016/j.gca.2006.06.1563>, 2006.
- 478 Loveless, A. J. and Russell, R. D.: A strong-focussing lens for mass spectrometer ion sources, *Int. J. Mass Spectrom. Ion Phys.*,  
479 3, 257–266, [https://doi.org/10.1016/0020-7381\(69\)85009-6](https://doi.org/10.1016/0020-7381(69)85009-6), 1969.
- 480 Mark, D. F., Barfod, D., Stuart, F. M., and Imlach, J.: The ARGUS multicollector noble gas mass spectrometer: Performance  
481 for  $^{40}\text{Ar}/^{39}\text{Ar}$  geochronology, *Geochem. Geophys. Geosystems*, 10, <https://doi.org/10.1029/2009GC002643>, 2009.
- 482 McDougall, I. and Harrison, T. M.: *Geochronology and Thermochronology by the  $^{40}\text{Ar}/^{39}\text{Ar}$  Method*, Oxford University  
483 Press., 1988.
- 484 McDougall, I. and Harrison, T. M.: *Geochronology and Thermochronology by the  $^{40}\text{Ar}/^{39}\text{Ar}$  Method, Second Edition.*,  
485 Oxford University Press, Oxford, New York, 282 pp., 1999.
- 486 Meunier, A., Velde, B., and Zalba, P.: Illite K-Ar dating and crystal growth processes in diagenetic environments: a critical  
487 review, *Terra Nova*, 16, 296–304, <https://doi.org/10.1111/j.1365-3121.2004.00563.x>, 2004.
- 488 Monié, P., Münch, P., Milesi, G., Bonno, M., and Iemmolo, A.:  $^{40}\text{Ar}/^{39}\text{Ar}$  geochronology of crustal deformation, *Comptes*  
489 *Rendus Géoscience*, 356, 1–29, <https://doi.org/10.5802/crgeos.209>, 2023.



- 490 Morgan, L. E., Postma, O., Kuiper, K. F., Mark, D. F., van der Plas, W., Davidson, S., Perkin, M., Villa, I. M., and Wijbrans,  
491 J. R.: A metrological approach to measuring  $^{40}\text{Ar}^*$  concentrations in K-Ar and  $^{40}\text{Ar}/^{39}\text{Ar}$  mineral standards: MEASURING  
492  $^{40}\text{Ar}^*$  CONCENTRATIONS, *Geochem. Geophys. Geosystems*, 12, n/a-n/a, <https://doi.org/10.1029/2011GC003719>, 2011.
- 493 Nier, A.: A Mass Spectrometer for Routine Isotope Abundance Measurements, *Rev. Sci. Instrum.*, 11, 212–216,  
494 <https://doi.org/doi:10.1063/1.1751688>, 1940.
- 495 Nier, A.: A Redetermination of the Relative Abundances of the Isotopes of Carbon, Nitrogen, Oxygen, Argon, and Potassium,  
496 *Phys. Rev.*, 77, 789–793, <https://doi.org/10.1103/PhysRev.77.789>, 1950.
- 497 Nomade, S.: Recommandation sur l'utilisation des unités de temps en sciences de la terre, *Quaternaire*, 28, 137–139,  
498 <https://doi.org/10.4000/quaternaire.7972>, 2017.
- 499 Odin, G. S.: Interlaboratory Standards for Dating Purposes, in: *Numerical dating in stratigraphy*, 123–148, 1982.
- 500 Peltz, M., Jacob, A., Grathoff, G. H., Enzmann, F., Kersten, M., and Warr, L. N.: A FIB-SEM Study of Illite Morphology in  
501 Aeolian Rotliegend Sandstones: Implications for Understanding the Petrophysical Properties of Reservoir Rocks, *Clays Clay  
502 Miner.*, 70, 84–105, <https://doi.org/10.1007/s42860-022-00174-9>, 2022.
- 503 Perry, E. A.: Diagenesis and the K-Ar Dating of Shales and Clay Minerals, *Geol. Soc. Am. Bull.*, 85, 827,  
504 [https://doi.org/10.1130/0016-7606\(1974\)85<827:DATKDO>2.0.CO;2](https://doi.org/10.1130/0016-7606(1974)85<827:DATKDO>2.0.CO;2), 1974.
- 505 Pevear, D. R.: Illite age analysis, a new tool for basin thermal history analysis, *International symposium on water-rock  
506 interaction*, 1251–1254, 1992.
- 507 Phillips, D., Matchan, E. L., Honda, M., and Kuiper, K. F.: Astronomical calibration of  $^{40}\text{Ar}/^{39}\text{Ar}$  reference minerals using  
508 high-precision, multi-collector (ARGUSVI) mass spectrometry, *Geochim. Cosmochim. Acta*, 196, 351–369,  
509 <https://doi.org/10.1016/j.gca.2016.09.027>, 2017.
- 510 van der Pluijm, B. A., Hall, C. M., Vrolijk, P. J., Pevear, D. R., and Covey, M. C.: The dating of shallow faults in the Earth's  
511 crust, *Nature*, 412, 172–175, <https://doi.org/10.1038/35084053>, 2001.
- 512 Poppe, L. J., Paskevich, V. F., Hathaway, J. C., and Blackwood, D. S.: *A Laboratory Manual for X-Ray Powder Diffraction.  
513 Procedures - Separation of the silt and clay fractions by centrifugation*, USGS, 2001.
- 514 Renne, P. R.: K-Ar and  $^{40}\text{Ar}/^{39}\text{Ar}$  Dating, in: *Quaternary Geochronology*, American Geophysical Union (AGU), 77–100,  
515 <https://doi.org/10.1029/RF004p0077>, 2000.
- 516 Renne, P. R., Cassata, W. S., and Morgan, L. E.: The isotopic composition of atmospheric argon and  $^{40}\text{Ar}/^{39}\text{Ar}$   
517 geochronology: Time for a change?, *Quat. Geochronol.*, 4, 288–298, <https://doi.org/10.1016/j.quageo.2009.02.015>, 2009.
- 518 Reuter, A. and Dallmeyer, R. D.: K-Ar and  $^{40}\text{Ar}/^{39}\text{Ar}$  dating of cleavage formed during very low-grade metamorphism: a  
519 review, *Geol. Soc. Lond. Spec. Publ.*, 43, 161–171, <https://doi.org/10.1144/GSL.SP.1989.043.01.10>, 1989.
- 520 Reynolds, R. C. and Thomson, C. H.: Illite from the Potsdam Sandstone of New York: A Probable Noncentrosymmetric Mica  
521 Structure, *Clays Clay Miner.*, 41, 66–72, <https://doi.org/10.1346/CCMN.1993.0410107>, 1993.
- 522 Rittmann, K. L.: Argon in Hornblende, Biotit und Muskovit bei der geologischen Abkühlung –  $^{40}\text{Ar}/^{39}\text{Ar}$  – Untersuchungen,  
523 Universität de Heidelberg, 1984.



- 524 Rouchon, V., Lefèvre, J.-C., Quidelleur, X., Guérin, G., and Gillot, P.-Y.: Nonspiked  $^{40}\text{Ar}$  and  $^{36}\text{Ar}$  quantification using a  
525 quadrupole mass spectrometer: A potential for K–Ar geochronology, *Int. J. Mass Spectrom.*, 270, 52–61,  
526 <https://doi.org/10.1016/j.ijms.2007.11.009>, 2008.
- 527 Rüdenauer, F. G.: Gas Scattering as a Limit to Partial-Pressure Sensitivity, *J. Vac. Sci. Technol.*, 9, 215–215,  
528 <https://doi.org/10.1116/1.1316557>, 1972.
- 529 Schaeffer, O. A. and Zähringer, J.: Potassium argon dating, Springer-Verlag, 278 pp., 1966.
- 530 Schwarz, W. H. and Trieloff, M.: Intercalibration of  $^{40}\text{Ar}$ – $^{39}\text{Ar}$  age standards NL-25, HB3gr hornblende, GA1550, SB-3,  
531 HD-B1 biotite and BMus/2 muscovite, *Chem. Geol.*, 242, 218–231, <https://doi.org/10.1016/j.chemgeo.2007.03.016>, 2007.
- 532 Snee, L. W., Sutter, J. F., and Kelly, W. C.: Thermochronology of economic mineral deposits; dating the stages of  
533 mineralization at Panasqueira, Portugal, by high-precision  $^{40}\text{Ar}/^{39}\text{Ar}$  age spectrum techniques on muscovite, *Econ. Geol.*, 83,  
534 335–354, <https://doi.org/10.2113/gsecongeo.83.2.335>, 1988.
- 535 Song, Y. and Sim, H.: Illite-Age-Analysis (IAA) for the Dating of Shallow Faults: Prerequisites and Procedures for  
536 Improvement, *Minerals*, 11, 1162, <https://doi.org/10.3390/min11111162>, 2021.
- 537 Śródoń, J. and Eberl, D. D.: Illite, in: 12. ILLITE, vol. 13, *Micas. Rev. Mineral*, 495–544,  
538 <https://doi.org/10.1515/9781501508820-016>, 1984.
- 539 Steiger, R. and Jäger, E.: Subcommittee on geochronology: convention on the use of decay constants in geo-and  
540 cosmochronology, *Earth Planet. Sci. Lett.*, 36, 359–362, 1977.
- 541 Turrin, B. D., Swisher, C. C., and Deino, A. L.: Mass discrimination monitoring and intercalibration of dual collectors in noble  
542 gas mass spectrometer systems, *Geochem. Geophys. Geosystems*, 11, <https://doi.org/10.1029/2009GC003013>, 2010.
- 543 Velde, B. and Meunier, A.: *The Origin of Clay Minerals in Soils and Weathered Rocks*, Springer Berlin Heidelberg, Berlin,  
544 Heidelberg, <https://doi.org/10.1007/978-3-540-75634-7>, 2008.
- 545 Viola, G., Torgersen, E., Mazzarini, F., Musumeci, G., Lelij, R., Schönenberger, J., and Garofalo, P. S.: New Constraints on  
546 the Evolution of the Inner Northern Apennines by K–Ar Dating of Late Miocene–Early Pliocene Compression on the Island of  
547 Elba, Italy, *Tectonics*, 37, 3229–3243, <https://doi.org/10.1029/2018TC005182>, 2018.
- 548 Werner, H. W.: A study on mass discrimination in a magnetic sector mass spectrometer, *Int. J. Mass Spectrom. Ion Phys.*, 14,  
549 189–203, [https://doi.org/10.1016/0020-7381\(74\)80007-0](https://doi.org/10.1016/0020-7381(74)80007-0), 1974.
- 550 Ylagan, R. F., Pevear, D. R., and Vrolijk, P. J.: Discussion of “Extracting K–Ar ages from shales: a theoretical test,” *Clay*  
551 *Miner.*, 35, 599–604, <https://doi.org/10.1180/000985500546918>, 2000.
- 552 Ylagan, R. F., Kim, C. S., Pevear, D. R., and Vrolijk, P. J.: Illite polytype quantification for accurate K–Ar age determination,  
553 *Am. Mineral.*, 87, 1536–1545, <https://doi.org/10.2138/am-2002-11-1203>, 2002.
- 554 Zwingmann, H., Clauer, N., and Gaupp, R.: Timing of fluid flow in a sandstone reservoir of the north German Rotliegend  
555 (Permian) by K–Ar dating of related hydrothermal illite, *Geol. Soc. Lond. Spec. Publ.*, 144, 91–106, 1998.

556